

10-5-2015


Temporal Variation in Optical Properties of Chromophoric Dissolved Organic Matter (CDOM) in Southern California Coastal Waters with Nearshore Kelp and Seagrass

Catherine D. Clark
Chapman University, cclark@chapman.edu

Warren J. De Bruyn
Chapman University, debruyn@chapman.edu

Paige Aiona
Chapman University

Follow this and additional works at: http://digitalcommons.chapman.edu/sees_articles

 Part of the [Biochemistry Commons](#), [Marine Biology Commons](#), [Oceanography Commons](#), [Organic Chemistry Commons](#), [Other Oceanography and Atmospheric Sciences and Meteorology Commons](#), and the [Terrestrial and Aquatic Ecology Commons](#)

Recommended Citation

Clark, C. D., De Bruyn, W. J. and Aiona, P. D. (2016), Temporal variation in optical properties of chromophoric dissolved organic matter (CDOM) in Southern California coastal waters with nearshore kelp and seagrass. *Limnol. Oceanogr.*, 61: 32–46. doi:10.1002/lno.10198

This Article is brought to you for free and open access by the Biology, Chemistry, and Environmental Sciences at Chapman University Digital Commons. It has been accepted for inclusion in Biology, Chemistry, and Environmental Sciences Faculty Articles and Research by an authorized administrator of Chapman University Digital Commons. For more information, please contact laughtin@chapman.edu.

Temporal Variation in Optical Properties of Chromophoric Dissolved Organic Matter (CDOM) in Southern California Coastal Waters with Nearshore Kelp and Seagrass

Comments

This article was originally published in *Limnology and Oceanography*, volume 61, in 2016. DOI: [10.1002/lno.10198](https://doi.org/10.1002/lno.10198)

Copyright

Association for the Sciences of Limnology and Oceanography

Temporal variation in optical properties of chromophoric dissolved organic matter (CDOM) in Southern California coastal waters with nearshore kelp and seagrass

Catherine D. Clark,^{†*} Warren J. De Bruyn, Paige D. Aiona

Department of Chemistry, School of Earth and Environmental Sciences, Schmid College of Science and Technology, Chapman University, Orange, California

Abstract

Optical properties of chromophoric dissolved organic matter (CDOM) were measured in surf zone waters in diurnal field studies at a Southern California beach with nearshore kelp and seagrass beds and intertidal plant wrack. Absorption coefficients ($a_{\text{CDOM}}(300 \text{ nm})$) ranged from 0.35 m^{-1} to 3.7 m^{-1} with short-term variability $< 1 \text{ h}$, increases at ebb and flood tides and higher values (6 m^{-1}) during an offshore storm event. Spectral slopes (S) ranged from 0.0028 nm^{-1} to 0.017 nm^{-1} , with higher values after the storm; S was generally inversely correlated with $a_{\text{CDOM}}(300 \text{ nm})$. 3-D excitation–emission matrix spectra (EEMs) for samples with lower S values had humic-type peaks associated with terrestrial material (A, C), marine microbial material (M) and protein peaks, characteristic of freshly produced organic material. Samples with high S values had no or reduced protein peaks, consistent with aged material. Fluorescent indexes ($f_{450}/f_{500} > 2.5$, $\text{BIX} > 1.1$) were consistent with microbial aquatic sources. Leachates of senescent kelp and seagrass had protein and humic-type EEM peaks. After solar simulator irradiation (4 h), protein peaks rapidly photochemically degraded, humic-type peak C increased in intensity and peak M disappeared. Optical characteristics of kelp leachates were most similar to field samples, consistent with minimal contributions from sea grass, a small component of the biomass at this site. Increases in $a_{\text{CDOM}}(300 \text{ nm})$ with decreases in S are attributed to the input of freshly produced autochthonous organic material at ebbing and flooding tides, from exudation and microbial processing of senescent plant wrack and nearshore macroalgal vegetation. Other allochthonous sources are hypothesized to be ground water seepage and terrestrial runoff.

Chromophoric dissolved organic matter (CDOM) plays an important role in determining light availability, biogeochemical cycling of carbon and ecosystem functioning in natural water systems (McKnight et al. 2001; Gallegos et al. 2005). CDOM in nearshore coastal regions typically derives from allochthonous inputs of terrestrial organic material from rivers, wetlands, estuaries, and salt marshes, with some contribution from in situ production by microbial and plankton communities (Steinberg et al. 2004; Stedmon and Markager 2005a,b; Romero-Castillo et al. 2010). There have been very limited studies to date on the contributions of intertidal and subtidal macroalgae and seagrass beds to CDOM production in coastal waters and no direct measurements of CDOM production from giant kelp (*Macrocystis pyrifera*), a species of

macroalgae which plays an important role in regional marine carbon cycles throughout the world.

Giant kelp beds, found in shallow temperate waters along the Pacific coast of North and South America, Africa, New Zealand, and Australia (Reed and Brzezinski 2009), are highly productive ecosystems which can export large quantities of biomass to adjacent ecosystems (Dugan et al. 2003). For example, Konotchik et al. (2012) recently estimated a daily average carbon production of $0.8\text{--}1.2 \text{ g C m}^{-2}$ for a large kelp bed off La Jolla in Southern California. Giant kelp is widely distributed in Pacific Ocean waters along the Southern California coast (see for example Stewart et al. 2009), with large amounts of wrack (hundreds of kilograms per meter per year) accumulating in the intertidal zone on un-groomed beaches (Dugan et al. 2003). In addition to standing kelp beds, there are thousands of large drifting rafts of kelp in the Southern California Bight which may strand on beaches (Hobday 2000). This marine macrophyte wrack supports an abundant and diverse biomass of macrofauna communities and shorebirds (Dugan et al. 2003).

*Correspondence: cclark@chapman.edu

[†]Present address: Department of Chemistry, College of Science and Engineering, Western Washington University, Bellingham, Washington

A few studies have indicated that aquatic plants, specifically seagrass and macroalgae, may be significant sources of CDOM in ocean regions which have limited freshwater inputs of organic matter from rivers and terrestrial runoff. Boss and Zaneveld (2003), in a study of tidally flushed shallow banks, showed that the inherent optical properties of the seawater had gradients over horizontal spatial scales and tidal timescales that were related to differences in biogeochemical processes occurring at bottom substrates. Remote sensing techniques were used to demonstrate the export of CDOM from seagrass beds on shallow banks in the Bahamas (Otis et al. 2004). The direct release of CDOM into seawater was shown in laboratory studies for exudates from 11 species of macroalgae (red, brown, and green algae) from temperate waters in the North Atlantic (Hulatt et al. 2009) and for seagrass (*Thalassia testudinum*) in chamber studies in subtropical South Florida waters (Stabenau et al. 2004). Swanson and Druehl (2002) showed that exudates of phlorotannins from the kelp species *Macrocystis integrifolia* attenuated artificial UVB radiation in seawater. Henderson et al. (2008) demonstrated the production of algal organic matter from four species of algae as part of the DOM pool in drinking water treatment processes.

Based on these prior studies, giant kelp should be an autochthonous CDOM source in coastal waters; at flood tide, inputs of exudates from kelp in nearshore beds would be brought to shore, whereas, at ebb tide, inputs from senescent plant wrack would be transported off shore, resulting in a temporal variation in optical properties. In regions with no significant fresh water inputs from rivers and rain events like Southern California with its semiarid Mediterranean climate, kelp may be a significant source of CDOM in coastal waters. Optical properties have been extensively used to assess CDOM sources and the extent and pathways of biogeochemical processing in seawater. For example, an analysis of trends in absorption coefficients, spectral slopes, and spectral slope ratios obtained from absorbance spectra provides information on relative molecular weight and aromaticity (Green and Blough 1994; Twardowski et al. 2004; Helms et al. 2008). In 3-D excitation–emission matrix (EEMs) fluorescence spectroscopy (see for example Coble et al. 1996; Stedmon et al. 2003, 2005; Murphy et al. 2008), peak locations have been used to differentiate CDOM as allochthonous senescent plant material or autochthonous biologically labile material (Moran and Zepp 1997; Miller et al. 2002; Tzortziou et al. 2007, 2011).

To examine CDOM sources, production and processing in coastal waters with nearshore giant kelp beds, we measured the optical properties of surf zone waters in multiple diurnal field studies at a beach in Southern California with extensive plant wrack in the intertidal zone and nearshore kelp and seagrass beds. Trends are analyzed on tidal timescales and the field results are compared to laboratory studies on giant

kelp and seagrass plant exudates which have undergone photochemical and biological processing.

Experimental methods

Site description

Four 24–28 h field studies were conducted in July 2009 at Crystal Cove Beach State Park (33.574 N 117.840 W) in Orange County, Southern California, U.S.A. on 7/1-2 (Field Study (FS) 1), 7/8-9 (FS 2), 7/15-16 (FS 3), and 7/29-30 (FS 4). The study site is shown in Fig. 1. Crystal Cove is one of the restoration sites of the Orange County Giant Kelp Restoration Project, begun in 2002 under the leadership of the Aquarium of the Pacific (Long Beach, California; http://www.aquariumofpacific.org/images/mcri_uploads/kelp_restoration_project.pdf). Eelgrass (*Zostera marina*), a type of seagrass native to Southern California, is found in meadows in shallow nearshore waters in this region (Allen and Williams 2003). There are now approximately 9000 m² of kelp (*M. pyrifera*) beds in the nearshore region spanning 1.6 km along the coastline. An additional 9000 m² was restored off Laguna Beach, which is located ~5 km down coast from our Crystal Cove study site. The kelp beds are 100–400 m offshore at depths of 7–12 m. Giant kelp canopy density is higher in summer (May–September) in Southern California (Gaylord et al. 2007; Stewart et al. 2009). No literature data on nearshore seagrass bed coverage is available for this site and region, but kelp dominated the intertidal zone based on relative wrack biomass (< 10% seagrass) over the study period.

Sampling methods

Samples were collected in 500 mL amber glass bottles every 60 min from knee-deep water on an incoming wave. Temperature was measured in situ. Samples were immediately vacuum filtered on site using 0.7 μm glass fiber filters (Whatman GFF) and stored in the dark at 4°C for analysis of optical properties at the laboratory within 48 h. Salinity and pH were measured in the laboratory with conductivity (Model 162A, Thermo ORION) and pH (Acument Basic AB15) meters. Sunlight intensity was measured in situ with a handheld UV light intensity radiometer/dosimeter with a built-in UV A + B photodiode sensor (VersaProbe, UV Process Supply). Over July, solar irradiance intensity reached a maximum of $4.7 \times 10^{-3} \text{ W cm}^{-2}$ during the day. A thick early morning fog layer, typical for this region at this time of year, delayed the onset of a solar radiation increase in some of the field studies for 2–3 h after sun-rise occurred around 6 am local time. Tidal data is from the United States Geological Service (USGS); no unusually high or low spring or neap tides were observed over the study period. Southern California experiences a semidiurnal tidal cycle, with two ebb and two flood tides of different magnitude occurring in each 24 h period. An offshore storm event resulted in high winds and strong longshore and rip currents during the first half of Study 4 (7/29-30). No rainfall was recorded during the study

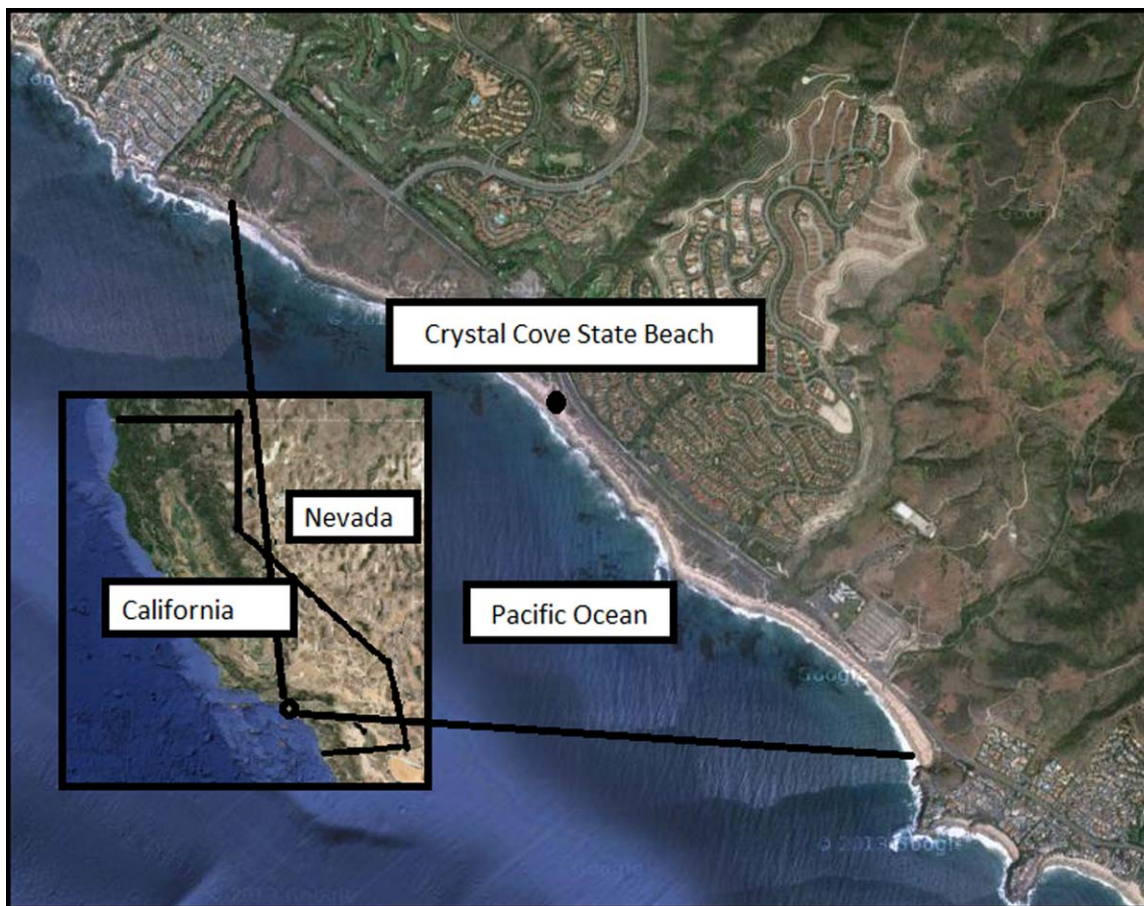


Fig. 1. Site map of study area at Crystal Cove State Beach, Orange County, Southern California, USA.

period (http://ocwatersheds.com/rainrecords/rainfalldata/historic_data/rainfall_data).

Optical properties

Absorbance spectra were measured with a UV-visible spectrometer (Agilent Technologies 8453) from 200 nm to 700 nm in a cylindrical quartz sample cell with a path length of 10 cm and a deionized water blank (Barnstead Nanopure). Spectral resolution was less than 2 nm with <0.03% stray light. Using Eq. 1, absorbance at 300 nm ($A(\lambda)$) was converted to absorption coefficient ($a_{\text{CDOM}}(300)$) in m^{-1} by multiplying by 2.303 (the natural logarithm of 10) and dividing by the cell path length L in m (Hu et al. 2002; Wozniak and Dera 2007).

$$a_{\text{CDOM}}(\lambda) = 2.303 A(\lambda)/L \quad (1)$$

Spectral slopes (S) were calculated by fitting the spectral data to Eq. 2 with a first-order linear regression for the 300–400 nm wavelength range for comparison to our previous work in this region (Clark et al. 2008, 2009, 2010, 2014):

$$a_{\text{CDOM}}(\lambda) = a_{\text{CDOM}}(\lambda_0) e^{-S(\lambda_0 - \lambda)} + K \quad (2)$$

where λ_0 is 300 nm and K is a background constant that allows for any baseline shift caused by residual scattering by fine particle size fractions, micro-air bubbles, or colloidal material present in the sample, refractive index differences between the sample and the reference, or attenuation not due to CDOM (Green and Blough 1994; Moran et al. 2000; Helms et al. 2008). The 100 nm range for S in this study appears to be well-fit by the linear regression method with $R^2 > 0.9$ (averaging 0.96 ± 0.06), except for the sample from FS 4 with the unusually high S value of 0.042 ($R^2 = 0.541$). Note that calculated slopes are negative with units of nm^{-1} , but absolute values are reported; a higher S value results from a steeper slope (more negative number) and gives a larger reported absolute value. Stedmon et al. (2000) reports a nonlinear approach is the best approach when calculating spectral slopes over broad spectral windows. However, Helms et al (2008) found less than 1% difference in S calculated using nonlinear exponential fits compared to the linear log-transformed values used in this study for smaller spectral windows. We report here results from using the linear

regression fit within the smaller spectral range of 300–400 nm to allow for the direct intercomparison of our results with other studies we have carried out and published in this region, but we also determined S values for our data using a nonlinear approach for comparison purposes. Values were generally similar with observed differences of $4 \pm 2\%$, $8 \pm 6\%$, $4 \pm 1\%$, and $6 \pm 4\%$ for all samples in field studies 1 through 4, respectively.

Emission spectra were obtained with a scanning fluorometer (Quantamaster, Photon Technology International). Three-dimensional EEMs were obtained by ranging the excitation wavelengths from 260 nm to 430 nm and the emission wavelengths from 270 nm to 650 nm in 5 nm increments. A water EEM was generated daily to subtract out the water Raman peak and Rayleigh scattering. Spectra were corrected for instrumental response using the correction file supplied by the manufacturer based on factory calibration. The percentage error on three duplicate absorbance and fluorescence scans was $<0.5\%$. Fluorescence intensities in photons s^{-1} were converted to QSU (quinine sulfate unit; 1 QSU = 1 ppb quinine sulfate in 0.05 M H_2SO_4) with a calibration curve (Mopper and Scultz 1993). Samples were diluted prior to fluorescence measurements to minimize inner filter effects as described in Burdige et al. (2004).

Two fluorescence indices were calculated following methods summarized in Huguet et al. (2010), specifically: f_{450}/f_{500} , the ratio of fluorescence intensities at 450 and 500 nm at an excitation of 370 nm, and BIX, the ratio of the intensities at 380 and 430 nm at an excitation of 310 nm.

Photodegradation experiments

To examine the contribution of kelp and seagrass as potential CDOM sources, we measured optical properties for plant leachates pre- and post-irradiation with a solar simulator. Senescent plant material, specifically giant kelp (*M. pyrifera*) and sea grass (*Z. marina*), was collected from the intertidal zone in May 2010, washed with deionized water and ~ 13 g immersed in 1.0 L of artificial seawater (aqueous NaCl solution; salinity 33). Live kelp from the nearshore beds could not be collected under the sampling permit restrictions. Samples were prepared with and without sodium azide to probe the effect of bacteria on CDOM generation. Duplicates were made up with the addition of 0.1% sodium azide (NaN_3) solution (Fisher Scientific) to the flask to kill bacteria. Flasks were placed in the dark at $22^\circ C$ for 24 h to dissolve optically active material formed in the senescent plants, and filtered under gentle vacuum through 0.7 μm glass fiber filters to remove large particulate material (Whatman). After filtration, solutions were stored at $4^\circ C$ in amber glass bottles wrapped in foil. A solar simulator (Luzchem Sol-Sim;) was used to irradiate samples in a quartz cell for a total of 4 h in 30 min intervals. The Luzchem Solar Simulator is calibrated to match the American Society for Testing and Materials (ASTM) Air Mass 1.5 Global Tilt Standard (AM1.5).

The simulator produces a spectrum that matches AM 1.5 within 80% from 280 through 680 nm both spectrally and in terms of intensity (http://www.luzchem.com/products/solar_sim.php). We irradiated samples for 4 h, to approximate the time-scale of maximum sun exposure over solar noon. EEMs were obtained pre- and post-irradiation with azide solution blanks and changes in the intensity and maximum excitation and emission wavelengths of the fluorescent peaks monitored. The $t = 0$ point was for the samples after 24 h of immersion, immediately before the irradiation experiment as conducted.

Results

Field study

Over the course of this study salinities ranged from 32 to 33, consistent with the low freshwater inputs coastal waters receive in this semiarid region with low rainfall (Clark et al. 2009). Average temperatures increased over the month of July, from $16.5 \pm 2.3^\circ C$ for the first study on 1–2 July to $23.8 \pm 0.5^\circ C$ for the last study at the end of July. Average temperatures for FS 2 and FS 3 were 20.1 ± 0.8 and $21.3 \pm 1.2^\circ C$, respectively. Over the same time period, the average pH increased from 8.2 ± 0.1 for FS 1 to 8.9 ± 0.1 for FS 4.

During field studies 1 through 3, the observed $a_{CDOM}(300\text{ nm})$ variability was contained within one order of magnitude with a minimum of 0.35 m^{-1} and a maximum of 3.7 m^{-1} . Fluctuations between low and high values occurred on subtidal time scales ranging from 1 h to 4 h (Fig. 2). Average values were 1.8 ± 0.6 , 1.3 ± 0.4 , and $1.7 \pm 0.5\text{ m}^{-1}$ for FS 1–3, respectively, ($n = 29$ for each field study). For FS 4, which occurred after a storm event, higher absorption coefficients ($4\text{--}6\text{ m}^{-1}$) were obtained for a few samples, but the overall average was similar to the three prior field studies ($1.7 \pm 1.7\text{ m}^{-1}$; $n = 20$). Increases were observed at both low and high tide minima and maxima heights, but also when changing from flood to ebb tide and between tidal minima and maxima. Similar CDOM absorption coefficient values of $1.5\text{--}2.0\text{ m}^{-1}$ were obtained in prior studies of coastal waters 5–10 km upcoast of this site (Clark et al. 2008, 2010).

Spectral slope values ranged from 0.0028 nm^{-1} to 0.017 nm^{-1} in the first three field studies, with temporal variability on the same timescale as $a(300)$ (Fig. 2). Average values were 0.004 ± 0.001 (FS1), 0.008 ± 0.002 (FS2), and 0.008 ± 0.002 (FS3) nm^{-1} . The overall average S value was slightly higher ($0.010 \pm 0.009\text{ nm}^{-1}$) for FS 4, due to higher values for some samples after the storm event (three samples with S values between 0.015 nm^{-1} and 0.020 nm^{-1} and one sample at 0.042 nm^{-1}). In prior studies at other beaches in this region, similar average S values in the range $0.010\text{--}0.0112\text{ nm}^{-1}$ were obtained (Clark et al. 2008). In general, a lower spectral slope was associated with a higher absorption coefficient (Fig. 3). In FS 1, which had the lowest average S value, the trend was flatter, with $a_{CDOM}(300\text{ nm})$ ranging

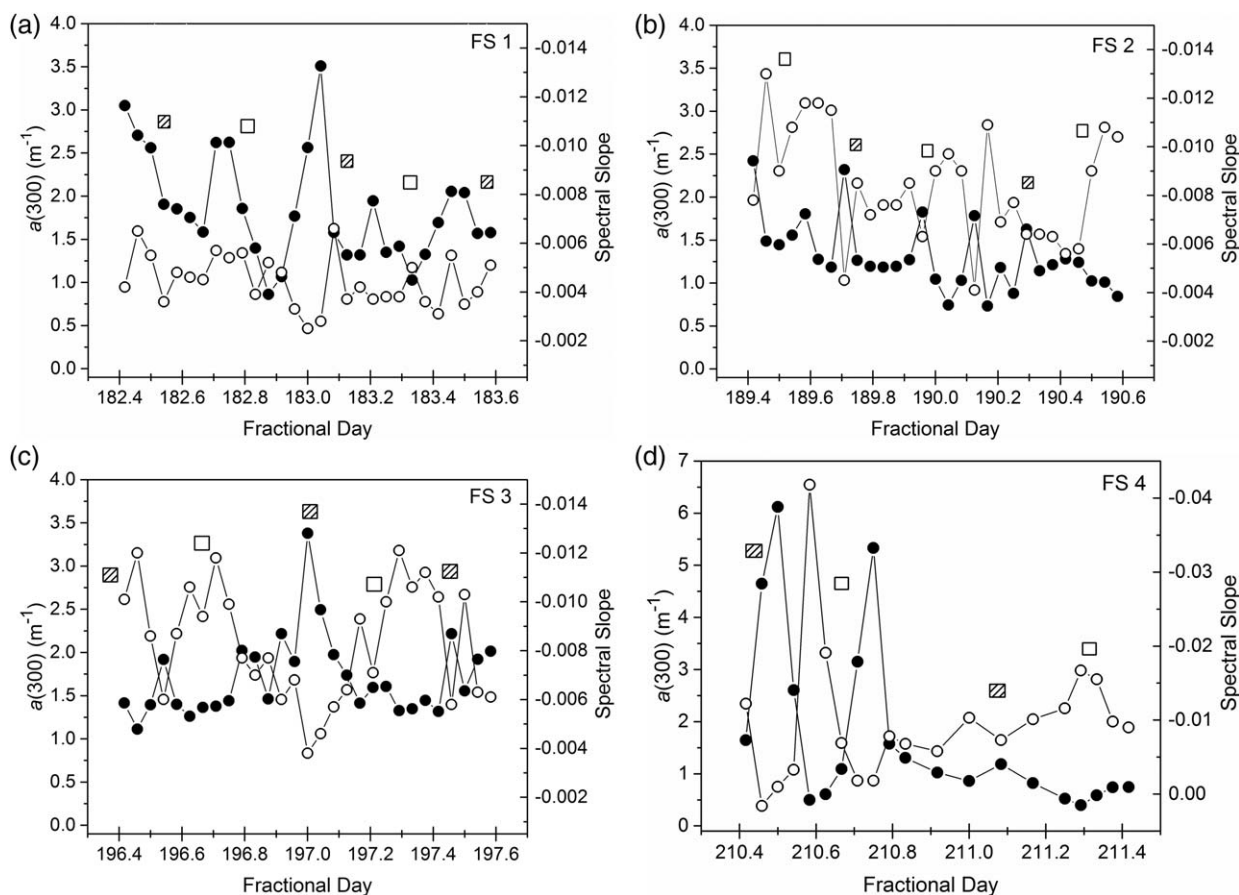


Fig. 2. Absorption coefficient ● ($a_{\text{CDOM}}(300 \text{ nm})$ in m^{-1}) and spectral slope ○ (in nm^{-1}) as a function of time for the 4 field studies (FS1–FS4). Time is given in fractional day of the year, where, for example, midday Feb 1 would be 32.5 in fractional days. Lines shown for ease of viewing. Locations of low and high tide height indicated by cross-hatched and open squares, respectively.

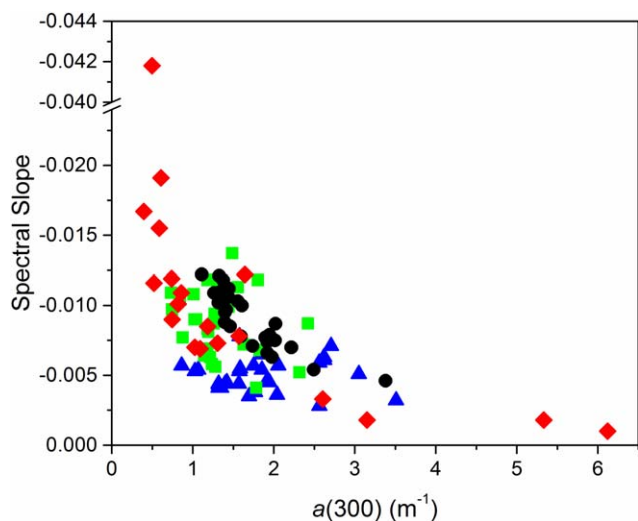


Fig. 3. Spectral slope vs. absorption coefficient ($a_{\text{CDOM}}(300 \text{ nm})$ in m^{-1}) for all samples from the four field studies: FS 1 blue ▲; FS 2 green ■; FS 3 black ●; FS 4 red ◆.

Table 1. Peak locations in 3-D excitation-emission matrix (EEM) spectra (from Coble 1996).

Peak name	Material type	Excitation maximum (nm)	Emission maximum (nm)
A	Humic-like	260	380–460
C	Terrestrial humic-like	350	420–480
M	Marine or microbial humic-like	312	380–420
T	Tryptophan protein-like	275	340
B	Tyrosine protein-like	275	310

from 1 m^{-1} to 3 m^{-1} for samples with similar spectral slopes of 0.0045 nm^{-1} .

To further examine CDOM optical properties, we measured EEMs for all samples. Three-dimensional EEMs have been shown to distinguish between CDOM sources in natural waters (Coble 1996; de Souza Sierra et al. 1997; McKnight et al. 2001). Five main fluorescent peaks were identified with

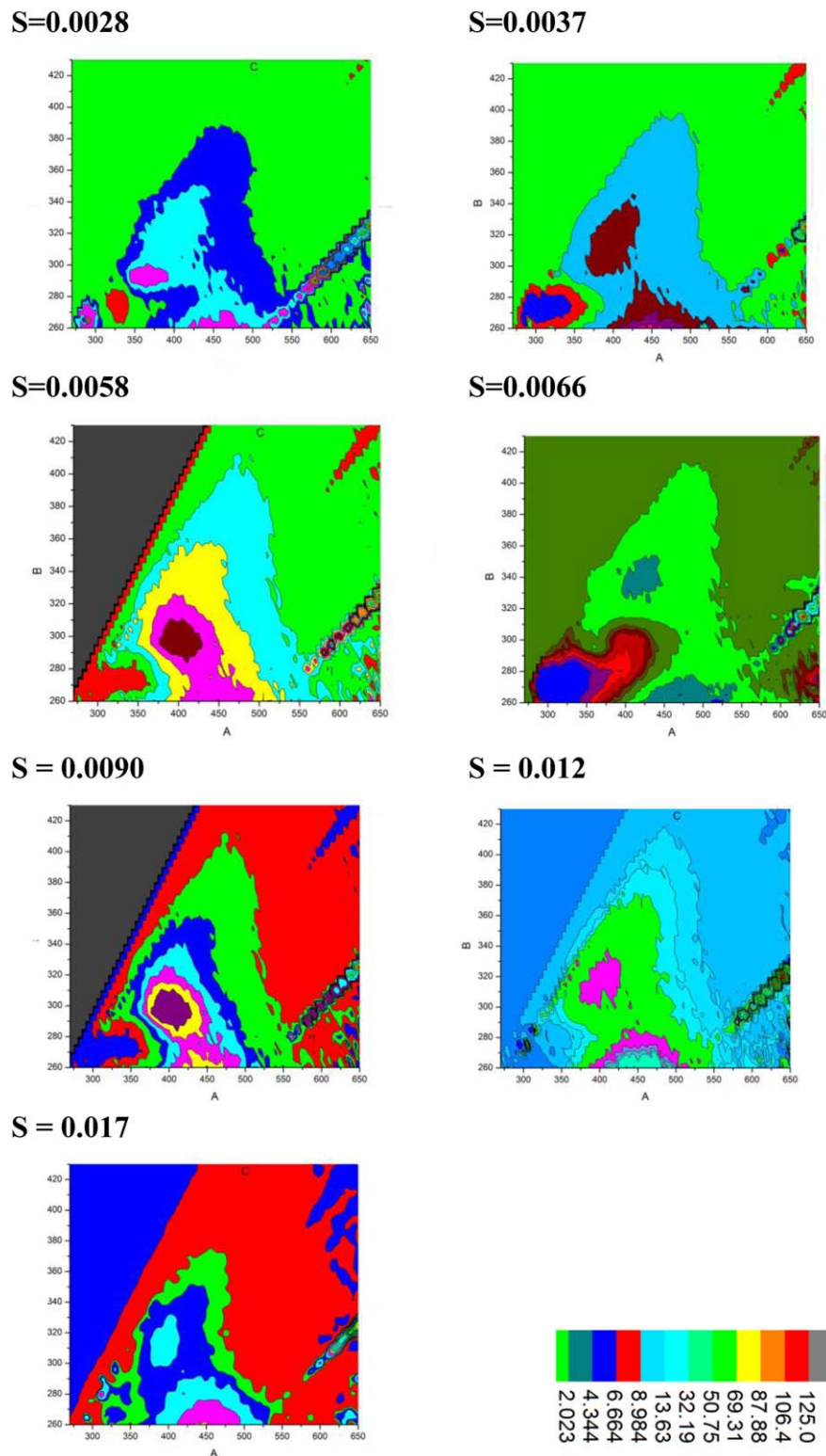


Fig. 4. Contour plots of representative 3D excitation–emission fluorescence matrices (EEMs) for a range of spectral slope values. Excitation wavelength (y -axis) vs. emission wavelength (x -axis) in nm. Fluorescence intensity scales (QSU) are 0–200 ($S = 0.0028$), 0–70 ($S = 0.0037$), 0–90 ($S = 0.0058$), 0–90 ($S = 0.0090$), 0–40 ($S = 0.012$), and 0–30 ($S = 0.017$).

distinct excitation and emission wavelength regions (Table 1); peak locations and classifications used here followed Coble (1996). Parallel factor analysis (PARAFAC), which can identify additional fluorescent components beyond the Coble model, was not used in this study due to the limited size of the spectral database ($n = 107$ from four field studies) available for fitting (PARAFAC models are typically on a much larger number of sample EEMs; Stedmon et al. 2003; Stedmon and Markager 2005; Murphy et al. 2008). EEMs are shown in Fig. 4 for water samples with spectral slope values ranging from 0.0028 nm^{-1} to 0.017 nm^{-1} . EEMs for the sample with the lowest spectral slope (0.0028 nm^{-1}) had two distinct protein peaks. Water samples with intermediate spectral slope ranges from 0.004 nm^{-1} to 0.009 nm^{-1} showed a single broad peak in the protein region. No protein peaks were observed for waters with higher spectral slopes ($> 0.012 \text{ nm}^{-1}$). Humic-type peaks A and C and microbial/marine-type peak M were observed in all samples.

The f_{450}/f_{500} index averaged 2.7 ± 0.02 for all the field studies. On a few occasions, values below two were obtained, for example 1.9 at midnight in FS 4 during a low tide. BIX values averaged 1.1 ± 0.1 for the four field studies; a high of 1.3 and a low of 0.9 were observed for some samples in FS 1/2 and FS 3/4, respectively. There was no significant correlation with absorption coefficient; for example, the highest f_{450}/f_{500} and BIX values (2.9 and 1.3, respectively) were observed for water samples with absorption coefficients ranging from 0.5 m^{-1} to 1.9 m^{-1} .

Photodegradation experiments

EEMs for seagrass and kelp leachates before and after irradiation for 4 h in the solar simulator are shown in Fig. 5. Figure 5 shows EEMs pre- and post-irradiation for leachates with the addition of sodium azide. Trends and changes in peak intensities are summarized in Table 2. Peaks A and C were observed at similar intensities (50 QSU) in both the seagrass and kelp leachates pre-irradiation with no added azide, i.e., in the presence of bacteria (Table 2). Since the absorption coefficient for the sea grass leachate was much higher than that for kelp (800% higher at 300 nm) for the same amount of plant material, this suggests that a large portion of the sea grass derived CDOM is not fluorescently active. Intense B and T protein peaks were observed for seagrass (1700 and 1200 QSU) whereas kelp had only one protein peak, the T peak, at a lower intensity of 300 QSU. When azide was added, peaks A and C were observed at similar intensities for the seagrass leachate but the protein peaks were not apparent. For kelp with azide pre-irradiation, peak T was again observed but at a lower intensity of 120 QSU, peak A was not apparent and peak C was observed at a similar intensity of 50 QSU (Table 2). Peak M was observed in the azide-treated kelp and seagrass leachates, i.e., in the absence of bacteria, at intensities in the same range as peaks A and C. We attribute the peak observed at an emission wavelength of 650 nm to pheophytins,

degraded chlorophyll pigments, from the senescent plant material (French et al. 1956). The emission wavelength range for peak C for the plant leachates in the laboratory studies was red-shifted by 40 nm compared to the field data (380–420 nm field vs. 420–480 nm leachates, respectively). This shift to longer wavelengths may be due to higher molecular weight, more freshly produced material for the leachates vs. more aged field material.

After irradiating the leachates without azide (i.e., in the presence of bacteria) for 4 h, protein peak intensities decreased for seagrass and kelp by factors of 5 and 2, respectively (Fig. 6). As the seagrass leachate was irradiated, the two distinct protein T and B peaks formed a single broader protein peak with lower intensity (Fig. 6). Peaks A and C doubled in intensity for kelp without azide post-irradiation; seagrass showed similar behavior for peak C but peak A intensity decreased by 40%. With the addition of azide (i.e., in the absence of bacteria), peak C for seagrass doubled in intensity to 130 QSU after irradiation, while peak A decreased to 15 QSU (Table 2). For kelp with azide post-irradiation, the T peak had decreased by 30% to 80 QSU and peak C increased slightly to 50 QSU.

Peak intensities for humic peaks A and C and protein peaks T and B are shown in Fig. 7 as a function of irradiation time for the leachates without azide; similar trends were observed for these peaks in the presence of azide (not shown). Peak M, which was only observed in azide-treated leachates, was rapidly photodegraded to non-detectable intensities by 30 min of irradiation time. Net rates for changes in fluorescent material derived from seagrass and kelp leachates were estimated from the relative change in QSU over the total irradiation time elapsed (4 h) to be 2.5 QSU h^{-1} for humic-type peak A photodegradation, $12\text{--}21 \text{ QSU h}^{-1}$ for humic-type peak C production, and $40\text{--}200 \text{ QSU h}^{-1}$ for protein peak T degradation (Table 2). The highest estimated decay rate was 380 QSU h^{-1} for protein peak B in seagrass without azide. The rapid complete photodegradation of peak M by 30 min gives an estimated photodegradation decay rate of $100\text{--}150 \text{ QSU h}^{-1}$.

Fluorescence indices were calculated for the plant leachates pre- and post-irradiation for 4 h with the solar simulator in the presence and absence of azide, i.e., without and with bacteria, respectively. The initial f_{450}/f_{500} ratio was similar for both kelp and seagrass with and without azide, averaging 1.1 ± 0.1 before irradiation and increasing to 2.0 ± 0.2 after irradiation. The BIX ratio showed more variability for both the leachates and azide conditions. For seagrass with azide, BIX values were low and unchanged pre- and post-irradiation (0.17 vs. 0.18). For kelp with azide, BIX was 0.97 before irradiation and increased to 1.5 after irradiation. Seagrass without azide had a higher BIX of 1.97 before irradiation which decreased to 0.52 after irradiation. By contrast, kelp without azide had a lower initial BIX value of 0.98 than seagrass, but a slightly higher post-irradiation value of 0.65.

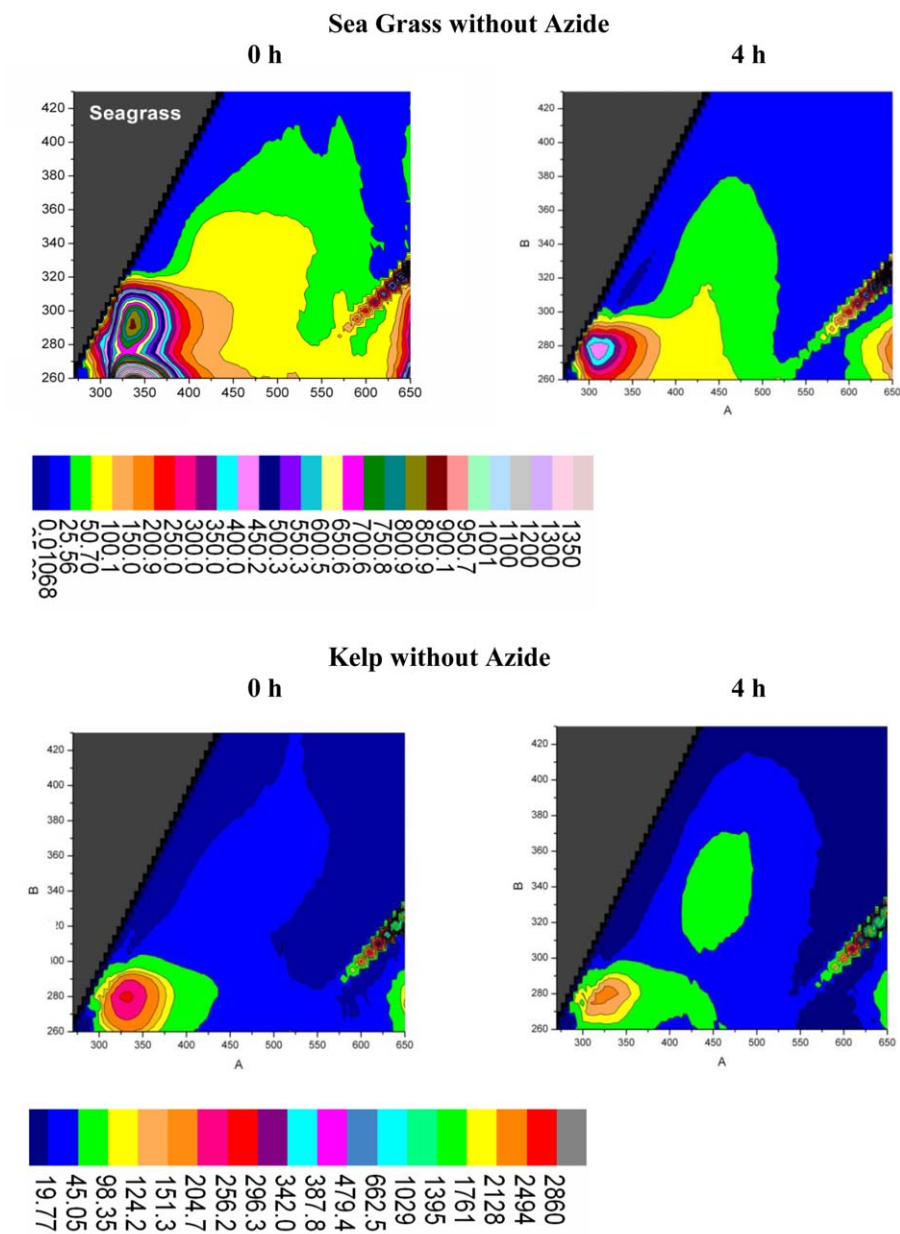


Fig. 5. Contour plots of 3D excitation-emission fluorescence matrices (EEMs) for kelp and seagrass leachates without azide at $t = 0$ and after 4 h of irradiation. Excitation wavelength (y -axis) vs. emission wavelength (x -axis) in nm. Fluorescence intensity scale is 0–1600 QSU for kelp and 0–1400 QSU for seagrass.

Discussion

Optical properties (like absorption coefficient, spectral slope, and fluorescence spectra) vary due to differences in the quantity, quality, and composition of CDOM, and can be used to examine the sources and biogeochemical processing of CDOM in natural water ecosystems.

We hypothesize the CDOM pool in nearshore coastal regions with limited freshwater riverine inputs consists of a combination of imported allochthonous material and autochthonous material produced in situ. Allochthonous

sources could include more freshly produced material from coastal salt marshes and estuarine systems and more aged material from upwelling of deeper waters and seepage from groundwater aquifers. Autochthonous sources would include production from plankton, diatoms, microbes, and aquatic plant material. Macroalgae could serve as a CDOM source either directly through leaching from senescent material or indirectly as exudates from biological processing. Increased nutrients in upwelled waters could also lead to enhanced autochthonous CDOM from increased plankton

Table 2. EEM peak intensities (in QSU) for kelp and seagrass leachates pre- and post-irradiation without and with the addition of azide; peak change rates (in QSU h⁻¹) are estimated from the change in intensity divided by the total irradiation time (4 h).

No azide	Seagrass					Kelp				
	A	C	M	B	T	A	C	M	B	T
Pre	25	50	n.o.	1700	1000	50	50	n.o.	n.o.	300
Post	15	135	n.o.	200*	200*	100	100	n.o.	n.o.	150
RATE	-2.5	+21		-380	-200	+12.5	+12.5			-37
+ azide										
Pre	25	60	75	n.o.	n.o.	n.o.	40	50	n.o.	120
Post	15	130	0	n.o.	n.o.	n.o.	50	0	n.o.	80
Rate	-2.5	+17	-150 [†]				+2.5	-100 [†]		-10

n.o.: not observed.

*Post-irradiation, peaks B and T combined into one peak.

[†]Time elapsed to 0 QSU was 0.5 h.

productivity. The CDOM sources which dominate in surf-zone waters would depend on water flow regimes. For example, CDOM on an outgoing ebb tide could arise from senescent plant material in the intertidal zone or seepage from groundwater aquifers, whereas inputs at flood tide could primarily be due to inputs from autochthonous sources in the nearshore region, like microbial and plankton production and macroalgae, or longshore transport of allochthonous material from up and downcoast marshes.

In this study, we observed increases in $a_{\text{CDOM}}(300 \text{ nm})$ at both high and low tides, consistent with multiple CDOM sources. Since we used GF/F glass fiber filters with a nominal pore size of $0.7 \mu\text{m}$ to remove particles from our seawater samples, some of the absorbance could potentially be due to bacteria and other particles small enough to pass through GF/F filters (Michaels and Knap 1996). The overall impact on optical properties depends on the levels of particles present. Some studies suggest the impacts of marine bacteria could be insignificant. For example, one study of marine bacteria gave estimated absorption coefficients of less than 0.001 m^{-1} (Stramski and Kiefer 1990), two orders of magnitude below the values of $0.5\text{--}4 \text{ m}^{-1}$ obtained in this study. Other studies have suggested that the impacts of marine bacteria could be more significant. Potential optical impacts include a peak at 400 nm and longer wavelength baseline offsets in the absorption spectra (Morel and Ahn 1990; Nelson et al. 1998), and characteristic peaks in the EEMS in the protein emission region (Determann et al. 1998). We do not see a 400 nm peak in our absorbance data and only one EEM showed any appreciable bacteria signal. The seagrass in the absence of azide, i.e., a leachate experiment with bacteria, show two peaks with an excitation at 290 and 240 nm and emission at 340 nm that could be due to bacteria (Determann et al. 1998). The longer wavelength baseline offset has a greater impact on the value of S if a long wavelength region (300–600 nm) is fitted, resulting in lower spectral slopes. Given that we fit the shorter wavelength region (300–400 nm) in

this study the impact of an offset should be minimal. Overall, while we cannot say with certainty that the use of $0.2 \mu\text{m}$ filters would not have produced optical differences, the data suggests that particulates, if present, were there in low levels and had minimal impact.

The S values in this study are similar to values previously reported for surface waters ebbing from an upcoast salt marsh ($0.010 \pm 0.002 \text{ nm}^{-1}$, Clark et al. 2008, 2014; GF/F and $0.2 \mu\text{m}$ filters, respectively), but lower than those typically reported for estuarine waters ($0.012\text{--}0.018 \text{ nm}^{-1}$; Vodacek et al. 1997; Burdige et al. 2004; Tzortziou et al. 2007). In a recent study, Helms et al. (2008) reported lower S values for upriver vs. coastal samples and observed an increase in S when water samples were irradiated with sunlight. Generally, S increases as CDOM is photobleached in oxidative environments and decreases with aging in suboxic soils and sediments due to increasing aromaticity and humification (Stabenau et al. 2004; Tzortziou et al. 2007). Lower S values are indicative of CDOM that is more humic or terrestrial in nature (Carder et al. 1989; Green and Blough 1994; Vodacek et al. 1997; Whitehead et al. 2000). The observed variations in spectral slope in this study suggest there are different CDOM types (due to source or processing) in these waters that can be differentiated based on optical properties.

We attribute the water with the highest S values ($> 0.015 \text{ nm}^{-1}$) to aged coastal seawater with CDOM that has undergone more extensive biological and photochemical processing. The single sample with $S = 0.40 \text{ nm}^{-1}$ from FS 4 may represent even more aged material brought into the nearshore region by winds and currents associated with the storm event, possibly from wind-driven upwelling processes (Snyder et al. 2003), but this had a low R^2 value of 0.5 for the S slope calculation and should be treated with caution. Material with mid-range S values ($0.006\text{--}0.012 \text{ nm}^{-1}$) is attributed to freshly produced material. The lowest S values ($0.002\text{--}0.003 \text{ nm}^{-1}$), observed at low tide during FS 1, could potentially be associated with seepage from groundwater

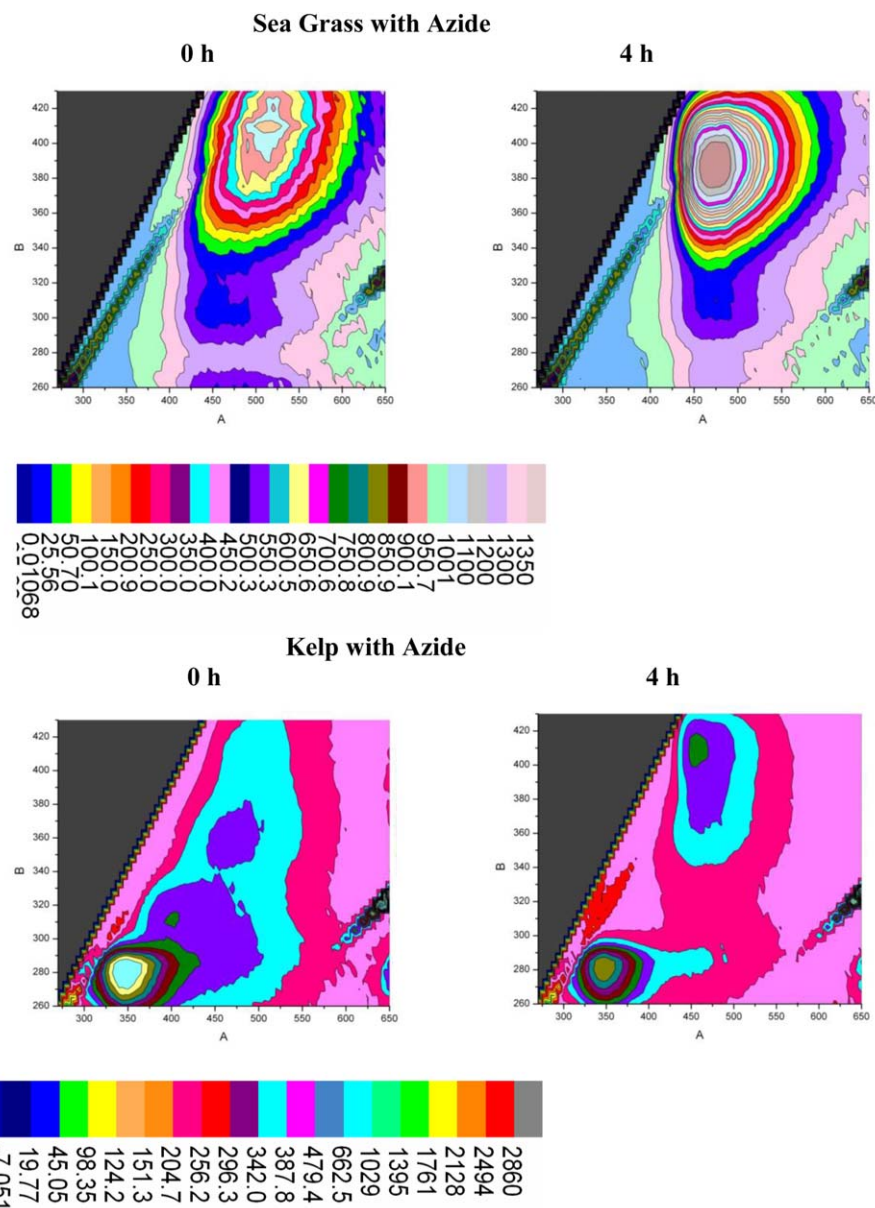


Fig. 6. Contour plots of 3D excitation-emission fluorescence matrices (EEMs) for kelp and seagrass leachates with azide at $t = 0$ and after 4 h of irradiation. Excitation wavelength (y -axis) vs. emission wavelength (x -axis) in nm. Fluorescence intensity scale is 0–300 QSU for kelp and 0–80 QSU for seagrass.

aquifers containing aged infiltrated material from runoff. The flux of groundwater to the surf zone from beach aquifers in this region has been previously reported (Boehm et al. 2006). We observed similar low S values in a prior study of deeper pore waters in sediments at an upcoast salt marsh (Clark et al. 2014).

In this study, increases in S (to a more negative slope or higher absolute value) were generally associated with decreases in $a_{\text{CDOM}}(300 \text{ nm})$; samples with the highest $a_{\text{CDOM}}(300 \text{ nm})$ had the lowest S values. The exception to this trend was for FS 1, which had a wide range of absorp-

tion coefficients associated with low spectral slope values. This could potentially be due to effects from upwelling, since the average temperature in this study was lower than the average of the other three field studies (16 vs. $22 \pm 2^\circ\text{C}$). Wind-driven upwelling leads to decreases in temperature and increases in productivity along the coast of California due to the transport of cold, nutrient rich water to the surface (Snyder et al. 2003); this could result in increased production of fresh material.

A similar inverse relationship between S and absorption coefficient was observed for a river and surrounding coastal

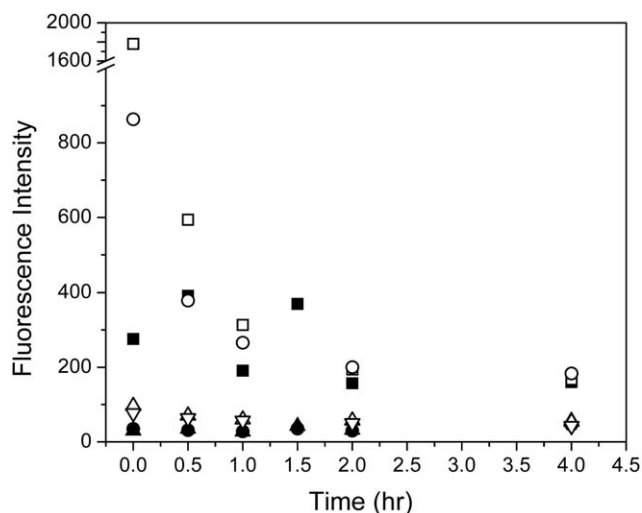


Fig. 7. Fluorescence intensity (QSU) vs. irradiation time (in h) for leachates of kelp (closed symbols) and seagrass (open symbols) without azide. Protein-type peaks: ● (peak T), ■ (peak B); humic-type peaks: ▲ (peak C), ▼ (peak A).

ocean in the South Atlantic Bight (Kowalczyk et al. 2003). The inverse trend in our study could be explained by the in situ production of fresh material in nearshore waters, hence lower S and higher $a_{\text{CDOM}}(300 \text{ nm})$. This CDOM may then be aged and diluted in seawater, resulting in higher S and lower $a_{\text{CDOM}}(300 \text{ nm})$. A recent study of intertidal and subtidal macroalgae exudates from coastal North Atlantic waters showed an increase of 0.004 in the spectral slope on photobleaching by sunlight over an exposure timescale of multiple days (Hulatt et al. 2009). Similar increases were observed in earlier studies of irradiated estuarine phytoplankton ($S_{\text{incr}} = 0.003 \text{ nm}^{-1}$ 10 d natural solar irradiation, St. Lawrence Estuary, Canada; Whitehead et al. 2000) and leachates of an Atlantic seagrass species ($S_{\text{incr}} = 0.001 \text{ nm}^{-1}$ 24 h solar simulator, Florida Bay, U.S.A.; Stabenau et al. 2004).

Peaks A, C, and M observed in EEMs for the water samples are attributed to a combination of humic material derived from terrestrial, microbial, and phytoplankton sources. Peak M has been associated with biological activity in seawater but has also been observed in wastewater, wetlands, salt-marshes, and agricultural environments in prior studies (Stedmon and Markager 2005a,b; Mostofa et al. 2007; Clark et al. 2008; Henderson et al. 2009). Romera-Castillo et al. (2010) demonstrated the production of peak M (and proteinaceous) material from exudation from four common species of marine phytoplankton, including diatoms. Peaks A and C are widespread, being observed in terrestrial, coastal, and oceanic waters, particularly the UV-humic like peak A (Stedmon and Markager 2005a; Mostofa et al. 2007; Clark et al. 2008). A prior study in this region showed that peak M material is produced in salt marshes, but absent in the adjacent receiving coastal waters, suggesting rapid biological and

photochemical processing and removal occurs (Clark et al. 2009). In laboratory incubation studies of leachates of salt marsh cord grass, peak M appeared to undergo biological conversion in the presence of bacteria (on the time-scale of days) to terrestrial-like humic material peak C (Wang et al. 2007).

Protein peaks were observed in water samples with lower spectral slopes, suggesting freshly produced material is present. The absence of protein peaks in waters with higher spectral slopes would be consistent with more aged and degraded material comprising the DOM pool. The protein-like peaks in EEMs have been associated with amino acids free or bound in proteins, with the tryptophan-like peak (T) indicating relatively recent origin or relatively unaltered DOM while peak B (tyrosine-like) indicates more degraded material (Yamashita and Tanoue 2003; Fellman et al. 2008). In a size exclusion chromatography study of CDOM in a coastal wetland and estuarine ecosystem, Maie et al. (2007) found that peak T consisted of two peaks, attributed to proteinaceous materials and polyphenols from tannins in senescent mangrove leaves. Stedmon and Markager (2005b) observed the production of protein-like fluorescent material during the exponential growth phase of phytoplankton.

The fluorescence indices provide additional evidence for potential CDOM sources. The f_{450}/f_{500} index provides an estimate of the degree of aromaticity; values of ~ 1.9 have been obtained for aquatic and microbial sources and ~ 1.3 for terrestrial and soil sources (McKnight et al. 2001). The average value of 2.7 ± 0.02 obtained in this study for FS 1 through 4 is consistent with aquatic and microbial sources. These conclusions are supported by the BIX index, a measure of autochthonous biological activity in estuarine and marine environments; higher values (> 1) are attributed to autochthonous DOM and OM freshly released in water, whereas lower values (0.6–0.7) are associated with lower in situ DOM production (Huguet et al. 2010). The average BIX value of 1.1 ± 0.1 for the four field studies is consistent with in situ production of fresh autochthonous DOM.

To assess potential autochthonous CDOM sources, and their biogeochemical processing, in coastal waters with extensive nearshore macroalgae, we measured optical properties and EEMs for leachates of kelp and sea grass collected at this site to compare to the natural water samples. The optical characteristics obtained from the non-azide experiments (with bacteria) should be comparable to those obtained during the field studies when both microbial and photochemical processing can occur. For the kelp leachate, the S value was 0.012 nm^{-1} pre-irradiation and 0.013 nm^{-1} post-irradiation for 4 h with the solar simulator, with a concomitant decrease of 7% in $a_{\text{CDOM}}(300 \text{ nm})$. By contrast, S for the sea grass leachate was higher at 0.024 nm^{-1} and decreased to 0.022 nm^{-1} after irradiation, with a slight increase of 3% in $a_{\text{CDOM}}(300 \text{ nm})$ after irradiation. An S value of 0.022 – 0.024 nm^{-1} was only observed for one point at the end of FS

4. In FS 2 and 3, the highest S values measured ranged from 0.011 nm^{-1} to 0.014 nm^{-1} between flood and ebb tides, comparable to the kelp leachate. In the second half of FS 4, after the major storm event, values were also fairly constant in the $0.011\text{--}0.014 \text{ nm}^{-1}$ range, with little tidal variability.

Both plant species produced CDOM with characteristics of terrestrial humic material and microbially produced material. Humic-type peak C was present in comparable intensities in kelp and seagrass in the absence of azide; this may be due to exudation from plant tissue. The production of UV-absorbing materials from a different species of kelp (*M. integrifolia*) has been attributed in a Canadian study to the release of phlorotannins (polyphenols) from plant tissues through exudation or cell damage, and subsequent reactions with proteinaceous and carbohydrate material in seawater (Swanson and Druehl 2002). For non-azide treated samples (i.e., with bacteria), intense protein-type peaks were observed for both seagrass and kelp. For seagrass without azide, the two intense protein-type peaks at an excitation of around 240 and 290 nm and emission of 340 nm for the leachate pre-irradiation may be due to bacteria (Determann et al. 1998). Post-irradiation, these features disappeared, possibly due to bacterial inactivation, to be replaced by a single peak with excitation at 275 nm and emission at 315 nm, characteristic of tyrosine and consistent with microbial processing. For kelp without azide, a single peak characteristic of tryptophan (excitation 280 nm, emission 330 nm) was observed pre- and post-irradiation. Peak M, attributed to CDOM of microbial origin, was not observed pre- or post-irradiation, possibly due to rapid biological processing. After irradiation with a solar simulator for 4 h, the protein-type peaks decreased in intensity by 50% for kelp and 80% for seagrass. Similar decreases of 70–80% were observed for protein peak intensities in a study of downstream river waters exposed to natural sunlight for 13 d (Mostofa et al. 2007). For both seagrass and kelp, peak C increased in intensity.

The azide-treated samples (i.e., no bacteria) had no protein peaks for seagrass and a lower intensity peak T for kelp, consistent with no or reduced microbial degradation. Seagrass had peaks A, C, and M pre-irradiation. Post-irradiation, peak A decreased in intensity, peak C doubled in intensity and peak M disappeared. Pre-irradiation, kelp had peaks C and M at similar intensities with no peak A. Post-irradiation, peak M had disappeared and peak C increased by 25% in intensity. For both leachates, peak M was rapidly photodegraded, disappearing by the first sampling point after 30 min of irradiation, as observed in a prior study on salt marsh plant leachates (Clark et al. 2008). The presence of peak M in the azide-treated samples prior to irradiation may be due to prior microbial production of material which persisted in the absence of biological processing.

Fluorescence indices for the plant leachates were consistent with the presence of a mixture of allochthonous terrestrial material (from plant exudation) and autochthonous

aquatic and microbial sources in the seawater. Values of f_{450}/f_{500} increased from 1.1 to 2.2 with irradiation for both plant leachates in the presence and absence of azide, suggesting that photochemical processes are producing material with the optical characteristics of aquatic CDOM, whether active microbes are present or not. The value post irradiation approaches the average value of 2.7 ± 0.02 obtained in this study for FS 1 through 4.

Results for the BIX ratio were less consistent. In the absence of azide (i.e., with bacteria), the BIX ratios > 1 before irradiation for kelp and seagrass were consistent with OM freshly released in water, as were the intense protein peaks observed in the EEMs. The value pre-irradiation for kelp of 0.98 compared most closely to the average BIX value of 1.1 ± 0.1 obtained for the four field studies; the value for seagrass was higher at 1.97. The lower values of 0.5–0.6 post-irradiation suggest reduced in situ CDOM microbial production occurs in the presence of sunlight, consistent with the observation of protein EEM peaks that decrease in intensity with irradiation. With azide, i.e., no active bacteria present, BIX ratios are very low for seagrass (< 0.2), consistent with no autochthonous microbial production of CDOM (as suggested by the absence of protein EEM peaks). The humic peaks observed in the seagrass EEMs would then be due to exudation of plant material. By contrast, BIX values for the azide-treated kelp leachate increased from ~ 1 to 1.5 with irradiation, consistent with CDOM production. This may be due to the fact that not all microbes on or in the kelp, a complex plant matrix, were deactivated with the azide treatment, which would be consistent with the fact that a reduced protein peak is still observed in the EEM for the kelp leachate with azide.

A combination of the EEMs for the azide and non-azide treated kelp leachates pre- and post-irradiation would have similar optical features to those observed in the field water samples, i.e., the presence of humic peaks A and C, peak M, and protein peaks. The higher relative intensity of peak A vs. C in the field samples as compared to the plant leachates suggest another allochthonous CDOM source, possibly from terrestrial inputs from run-off from storm water drains or groundwater seepage.

In summary, the temporal variation in the optical characteristics of coastal waters with limited freshwater riverine inputs and extensive nearshore macroalgal vegetation are consistent with multiple potential allochthonous and autochthonous CDOM sources. Autochthonous sources include exudation from and microbial processing of plant wrack in the intertidal zone and actively growing macroalgal plants offshore. Increased absorption coefficients and decreased spectral slopes observed at both ebb and flood tides were consistent with production of fresh CDOM under both tidal conditions. The presence of protein peaks and peak M in EEMs of water samples is consistent with microbial production occurring. Leachates of kelp with active

microbial populations pre- and post-irradiation had the most similar optical features to the coastal water samples, as compared to sea grass.

References

- Allen, B. J., and S. L. Williams. 2003. Native eelgrass *Zostera marina* controls growth and reproduction of an invasive mussel through food limitation. *Mar. Ecol. Prog. Ser.* **254**: 57–67.
- Boehm, A. B., A. Paytan, G. G. Shellenberger, and K. A. Davis. 2006. Composition and flux of groundwater from a California beach aquifer: Implications for nutrient supply to the surf zone. *Cont. Shelf Res.* **26**: 269–282. doi:10.1016/j.csr.2006.01.005
- Boss, E. and J. R. Zaneveld. 2003. The effect of bottom substrate on inherent optical properties: Evidence of biogeochemical processes. *Limnol. Oceanogr.* **48**: 346–354. doi:10.4319/lo.2003.48.1_part_2.0346
- Burdige, D. J., S. W. Kline, and W. Chen. 2004. Fluorescent dissolved organic matter in marine sediment porewaters. *Mar. Chem.* **89**: 289–311. doi:10.1016/j.marchem.2004.02.015
- Carder, K. L., R. G. Steward, G. R. Harvey, and P. B. Ortner. 1989. Marine humic and fulvic acids: Their effects on remote sensing of chlorophyll. *Limnol. Oceanogr.* **34**: 68–81. doi:10.4319/lo.1989.34.1.0068
- Clark, C. D., L. P. Litz, and S. B. Grant. 2008. Saltmarshes as a source of chromophoric dissolved organic matter to Southern California coastal waters. *Limnol. Oceanogr.* **53**: 1923–1933. doi:10.4319/lo.2008.53.5.1923
- Clark, C. D., W. J. De Bruyn, and J. G. Jones. 2009. Photochemical production of hydrogen peroxide in size-fractionated Southern California coastal waters. *Chemosphere* **76**: 141–146. doi:10.1016/j.chemosphere.2009.01.076
- Clark, C. D., W. J. De Bruyn, C. B. Hirsch, and S. D. Jakubowski. 2010. Spatial and temporal measurements of hydrogen peroxide concentrations in recreational marine bathing waters in Southern California. *Water Res.* **44**: 2203–2210. doi:10.1016/j.watres.2009.12.044
- Clark, C. D., P. Aiona, J. Keller, and W. J. De Bruyn. 2014. Optical characterization and distribution of chromophoric dissolved organic matter (CDOM) in soil porewater from a salt marsh ecosystem. *Mar. Ecol. Prog. Ser.* **516**: 71–83.
- Coble, P. G. 1996. Characterization of marine and terrestrial DOM in seawater using excitation emission matrix spectroscopy. *Mar. Chem.* **51**: 325–346. doi:10.1016/0304-4203(95)00062-3
- De Souza Sierra, M. M., O. F. X. Donard, and M. Lamotte. 1997. Spectra identification and behavior of dissolved organic fluorescent material during estuarine mixing processes. *Mar. Chem.* **58**: 51–58. doi:10.1016/S0304-4203(97)00025-X
- Dekker, A. G., V. E. Brando, and J. M. Anstee. 2005. Restrospective seagrass change detection in a shallow coastal tidal Australian lake. *Remote Sens. Environ.* **97**: 415–433. doi:10.1016/j.rse.2005.02.017
- Determann, S., J. M. Lobbes, R. Reuter, and J. Rullkotter. 1998. Ultraviolet fluorescence excitation and emission spectroscopy of marine algae and bacteria. *Mar. Chem.* **62**: 137–156. doi:10.1016/S0304-4203(98)00026-7
- Dugan, J. E., D. M. Hubbard, M. D. McCrary, and M. O. Pierson. 2003. The response of macrofauna communities and shore birds to macrophyte wrack subsidies on exposed sandy beaches of southern California. *Estuar. Coast. Shelf Sci.* **58S**: 25–40. doi:10.1016/S0272-7714(03)00045-3
- Fellman, J. B., D. V. D'Amore, E. Hood, and R. D. Boone. 2008. Fluorescence characteristics and biodegradability of dissolved organic matter in forest and wetland soils from coastal temperate watersheds in southeast Alaska. *Biogeochemistry* **88**: 169–184. doi:10.1007/s10533-008-9203-x
- Gallegos, C. L., T. E. Jordan, A. H. Hines, and D. E. Weller. 2005. Temporal variability of optical properties in a shallow, eutrophic estuary: Seasonal and interannual variability. *Estuar. Coast. Shelf Sci.* **64**: 156–170. doi:10.1016/j.ecss.2005.01.013
- Gaylord, B., and others. 2007. Spatial patterns of flow and their modification within and around a giant kelp forest. *Limnol. Oceanogr.* **52**: 1838–1852. doi:10.4319/lo.2007.52.5.1838
- Green, S. A., and N. V. Blough. 1994. Optical absorption and fluorescence properties of chromophoric dissolved organic matter in natural waters. *Limnol. Oceanogr.* **39**: 1903–1916. doi:10.4319/lo.1994.39.8.1903
- Helms, J. R., A. Stubbins, J. D. Ritchie, E. C. Minor, D. J. Kieber, and K. Mopper. 2008. Absorption spectral slopes and slope ratios as indicators of molecular weight, source, and photobleaching of chromophoric dissolved organic matter. *Limnol. Oceanogr.* **53**: 955–969. doi:10.4319/lo.2008.53.3.0955
- Henderson, R. K., A. Baker, S. A. Parsons, and B. Jefferson. 2008. Characterization of algogenic organic matter extracted from cyanobacteria, green algae and diatoms. *Water Res.* **42**: 3435–3445. doi:10.1016/j.watres.2007.10.032
- Hobday, A. 2000. Persistence and transport of fauna on drifting kelp (*Macrocystis pyrifera*) rafts in the Southern California Bight. *J. Exp. Mar. Biol. Ecol.* **253**: 75–96. doi:10.1016/S0022-0981(00)00250-1
- Hu, C., F. E. Muller-Karger, and R. G. Zepp. 2002. Absorbance, a(300) and apparent quantum yield: A comment on common ambiguity in the use of these optical concepts. *Limnol. Oceanogr.* **47**: 1261–1267. doi:10.4319/lo.2002.47.4.1261
- Huguet, A., and others. 2010. New insights into the size distribution of fluorescent dissolved organic matter in estuarine waters. *Org. Geochem.* **41**: 595–610. doi:10.1016/j.orggeochem.2010.02.006
- Hulatt, C. J., D. N. Thomas, D. G. Bowers, L. Norman, and C. Zhang. 2009. Exudation and decomposition of chromophoric dissolved organic matter (CDOM) from some temperate macro algae. *Estuar. Coast. Shelf Sci.* **84**: 147–153. doi:10.1016/j.ecss.2009.06.014
- Konotchick, T., P. E. Parnell, P. K. Dayton, and J. J. Leichter. 2012. Vertical distribution of *Macrocystis pyrifera* nutrient

- exposure in southern California. *Estuar. Coast. Shelf Sci.* **106**: 85–92. doi:10.1016/j.ecss.2012.04.026
- Kowalczyk, P., W. J. Cooper, R. F. Whitehead, M. J. Durako, and W. Sheldon. 2003. Characterization of CDOM in an organic-rich river and surrounding coastal ocean in the South Atlantic Bight. *Aquat. Sci.* **65**: 384–401. doi:10.1007/s00027-003-0678-1
- Maie, N., N. M. Scully, O. Pisani, and R. Jaffe. 2007. Composition of a protein-like fluorophore of dissolved organic matter in coastal wetland and estuarine ecosystems. *Water Res.* **41**: 563–570. doi:10.1016/j.watres.2006.11.006
- McKnight, D. M., E. W. Boyer, P. K. Westerhoff, P. T. Doran, T. Kulbe, and D. T. Andersen. 2001. Spectrofluorometric characterization of dissolved organic matter for indication of precursor organic material and aromaticity. *Limnol. Oceanogr.* **46**: 38–48. doi:10.4319/lo.2001.46.1.0038
- Michaels, A. F., and A. H. Knap. 1996. Overview of the US JGOFs Bermuda Atlantic time-series study and the hydrostation S program. *Deep-Sea Res. II* **43**: 157–198. doi:10.1016/0967-0645(96)00004-5
- Mopper, K., and C. A. Schultz. 1993. Fluorescence as a possible tool for studying the nature and water column distribution of DOC components. *Mar. Chem.* **41**: 229–238. doi:10.1016/0304-4203(93)90124-7
- Moran, M. A., and R. G. Zepp. 1997. Role of photoreactions in the formation of biologically labile compounds from dissolved organic matter. *Limnol. Oceanogr.* **42**: 1307–1316. doi:10.4319/lo.1997.42.6.1307
- Moran, M. A., W. M. Sheldon, and R. G. Zepp. 2000. Carbon loss and optical property changes during long-term photochemical and biological degradation of estuarine dissolved organic matter. *Limnol. Oceanogr.* **45**: 1254–1264. doi:10.4319/lo.2000.45.6.1254
- Morel, A., and Y.-H. Ahn. 1990. Optical efficiency of free-living marine bacteria: Influence of bacterioplankton upon the optical properties and particulate organic carbon in oceanic waters. *J. Mar. Res.* **48**: 145–175. doi:10.1357/002224090784984632
- Mostafa, K. M. G., T. Yoshioka, E. Konohiro, and E. Tanoue. 2007. Photodegradation of fluorescent dissolved organic matter in river waters. *Geochem. J.* **41**: 323–331. doi:10.2343/geochemj.41.323
- Murphy, K. R., C. A. Stedmon, T. D. Waite, and G. M. Ruiz. 2008. Distinguishing between terrestrial and autochthonous organic matter sources in marine environments using fluorescence spectroscopy. *Mar. Chem.* **108**: 40–58. doi:10.1016/j.marchem.2007.10.003
- Nelson, N. B., D. A. Siegel, and A. F. Michaels. 1998. Seasonal dynamics of colored dissolved material in the Sargasso Sea. *Deep-Sea Res.* **45**: 931–957. doi:10.1016/S0967-0637(97)00106-4
- Otis, D. B., K. L. Carder, D. C. English, and J. E. Ivey. 2004. CDOM transport from the Bahama Banks. *Coral Reefs* **23**: 152–160. doi:10.1007/s00338-003-0356-8
- Reed, D., and M. A. Brzezinski. 2009. Kelp forests. In D. Laffoley, and G. D. Grimsditch [eds.], *The management of natural carbon sinks*. International Union for Conservation of Nature and Natural Resources.
- Romera-Castillo, C., H. Sarmento, X. A. Alvarez-Salgado, J. M. Gasol, and C. Marrasse. 2010. Production of chromophoric dissolved organic matter by marine phytoplankton. *Limnol. Oceanogr.* **55**: 446–454. doi:10.4319/10.2010.55.1.0446
- Snyder, M. A., L. C. Sloan, N. S. Diffenbaugh, and J. L. Bell. 2003. Future climate change and upwelling in the California Current. *Geophys. Res. Lett.* **30**: 1832. doi:10.1029/2002PA000865
- Stabenau, E. R., R. G. Zepp, E. Bartels, and R. G. Zika. 2004. Role of the seagrass *Thalassia testudinum* as a source of chromophoric dissolved organic matter in coastal South Florida. *Mar. Ecol. Prog. Ser.* **282**: 59–72. doi:10.3354/meps282059
- Stedmon, C. A., S. Markager, and R. Bro. 2003. Tracing dissolved organic matter in aquatic environments using a new approach to fluorescence spectroscopy. *Mar. Chem.* **82**: 219–254. doi:10.1016/S0304-4203(03)00072-0
- Stedmon, C. A., and S. Markager. 2005a. Resolving the variability in dissolved organic matter fluorescence in a temperate estuary and its catchment using PARAFAC analysis. *Limnol. Oceanogr.* **50**: 686–697. doi:10.4319/lo.2005.50.2.0686
- Stedmon, C. A., and S. Markager. 2005b. Tracing the production and degradation of autochthonous fractions of dissolved organic matter by fluorescence analysis. *Limnol. Oceanogr.* **50**: 1415–1426. doi:10.4319/lo.2005.50.5.1415
- Steinberg, D. K., N. B. Nelson, C. A. Carson, and A. C. Prusak. 2004. Production of chromophoric dissolved organic matter (CDOM) in the open ocean by zooplankton and the colonial cyanobacterium *Trichodesmium* spp. *Mar. Ecol. Prog. Ser.* **267**: 45–56. doi:10.3354/meps267045
- Stewart, H. L., J. P. Fram, D. C. Reed, S. L. Williams, M. A. Brzezinski, S. MacIntyre, and B. Gaylord. 2009. Differences in growth, morphology and tissue carbon and nitrogen of *Macrocystis pyrifera* within and at the edge of a giant kelp forest in California, USA. *Mar. Ecol. Prog. Ser.* **375**: 101–112. doi:10.3354/meps07752
- Stramski, D., and D. A. Kiefer. 1990. Optical properties of marine bacteria. *Ocean Optics X, Proc. S.P.I.E.* **1302**: 250–268. doi:10.1117/12.21450
- Swanson, A. K., and L. D. Druehl. 2002. Induction, exudation and the UV protective role of kelp phlorotannins. *Aquat. Bot.* **73**: 241–253. doi:10.1016/S0304-3770(02)00035-9
- Tzortziou, M., C. L. Osburn, and P. J. Neale. 2007. Photo-bleaching of dissolved organic material from a tidal marsh-estuarine system of the Chesapeake Bay. *Photochem. Photobiol.* **83**: 782–792. doi:10.1111/j.1751-1097.2007.00142.x
- Tzortziou, M., P. J. Neale, J. P. Megonigal, C. L. Pow, and M. Butterworth. 2011. Spatial gradients in dissolved organic

- carbon due to tidal marsh outwelling into a Chesapeake Bay estuary. *Mar. Ecol. Prog. Ser.* **426**: 41–56. doi: [10.3354/meps09017](https://doi.org/10.3354/meps09017)
- Vodacek, A., N. V. Blough, M. D. DeGrandpre, E. T. Peltzer, and R. K. Nelson. 1997. Seasonal variation of CDOM and DOC in the Middle Atlantic Bight: Terrestrial inputs and photooxidation. *Limnol. Oceanogr.* **42**: 674–686. doi: [10.4319/lo.1997.42.4.0674](https://doi.org/10.4319/lo.1997.42.4.0674)
- Wang, X.-C., L. Litz, R. F. Chen, W. Huang, P. Feng, and M. A. Altabet. 2007. Release of dissolved organic matter during oxic and anoxic decomposition of salt marsh cordgrass. *Mar. Chem.* **105**: 309–321. doi:[10.1016/j.marchem.2007.03.005](https://doi.org/10.1016/j.marchem.2007.03.005)
- Whitehead, R. F., S. de Mora, S. Demers, M. Gosselin, P. Monfort, and B. Mostajir. 2000. Interactions of ultraviolet-B radiation, mixing and biological activity on photobleaching of natural chromophoric dissolved organic matter: A mesocosm study. *Limnol. Oceanogr.* **45**: 278–291. doi:[10.4319/lo.2000.45.2.0278](https://doi.org/10.4319/lo.2000.45.2.0278)
- Wozniak, B., and J. Dera. 2007. Light absorption in seawater. Springer.
- Yamashita, Y., and T. Tanoue. 2003. Chemical characterization of protein-like fluorophores in DOM in relation to aromatic amino acids. *Mar. Chem.* **82**: 255–271. doi: [10.1016/S0304-4203\(03\)00073-2](https://doi.org/10.1016/S0304-4203(03)00073-2)

Acknowledgments

CDC and WJD thank the National Science Foundation (OCE grant #072528433) for support. The authors thank undergraduate students Charlie Hirsch and Benjamin Brahm for assistance with sampling. We also thank Harry Helling of the Crystal Cove Alliance and Crystal Cove State Park for site access and use of the marine research facility.

Submitted 19 January 2015

Revised 20 May 2015, 7 July 2015

Accepted 27 July 2015

Associate editor: Anna Romani